SOLAR SAIL ATTITUDE CONTROL PERFORMANCE COMPARISON

Jeff J. Bladt* and Dale A. Lawrence**

Performance of two solar sail attitude control implementations is evaluated. One implementation employs four articulated reflective vanes located at the periphery of the sail assembly to generate control torque about all three axes. A second attitude control configuration uses mass on a gimbaled boom to alter the center-of-mass location relative to the center-of-pressure producing roll and pitch torque along with a pair of articulated control vanes for yaw control. Command generation algorithms employ linearized dynamics with a feedback inversion loop to map desired vehicle attitude control torque into vane and/or gimbal articulation angle commands. We investigate the impact on actuator deflection angle behavior due to variations in how the Jacobian matrix is incorporated into the feedback inversion loop. Additionally, we compare how well each implementation tracks a commanded thrust profile, which has been generated to follow an orbital trajectory from the sun-earth L1 point to a sub-L1 station.

INTRODUCTION

Solar sails are envisioned as effective spacecraft propulsion devices requiring no on-board propellant. Solar sail technologies and mission concepts have been studied and developed for many years[1,2]. Sailcraft mission concepts include planetary exploration of the inner and outer solar system, out-of-ecliptic flight paths for studying solar polar activity, and non-Keplerian trajectories such as sub-L1 halo orbits to monitor space weather and provide early warning for protecting terrestrial infrastructure. NASA's In-Space Propulsion (ISP) Technology Office has supported recent development efforts that include mission design[3,4], vehicle design[5,6], and guidance, navigation, & control[7,8,9]. Solar sail flight system technology development is a candidate for NASA's New Millennium Program (NMP) Space Technology-9 mission[10].

Designing solar sail missions requires a high-fidelity simulation and modeling tool set that integrates guidance, navigation, and control (GN&C) functions. Integrated GN&C modeling is crucial to accurately predict solar sail dynamic performance because there is coupling between sailcraft attitude and thrust. Thrust is induced on a solar sail by the momentum exchange of reflected and absorbed solar photons on the sail surface. The thrust vector (i.e., magnitude and

* Ball Aerospace & Technologies Corp., P.O. Box 1062, Boulder, CO 80306
** Associate Professor, Department of Aerospace Engineering Sciences, University of Colorado, Boulder, CO 80309

direction) is a function of the sail assembly's attitude relative to the sun-to-sailcraft line, and so solar sail orbital trajectory control cannot be decoupled from sailcraft attitude control.

NASA's In-Space Propulsion Office has awarded a study contract to develop a Solar Sail Spaceflight Simulation Software (S5) Toolkit, and the study is led by JPL with teammates from academia, government, and industry[11]. S5 is coded in object oriented C++ with a Python scripting layer for customization, a MATLAB interface for plotting capabilities, and a graphical user interface. Figure 1 illustrates a functional block diagram of the sailcraft integrated GN&C simulation tool currently under development.

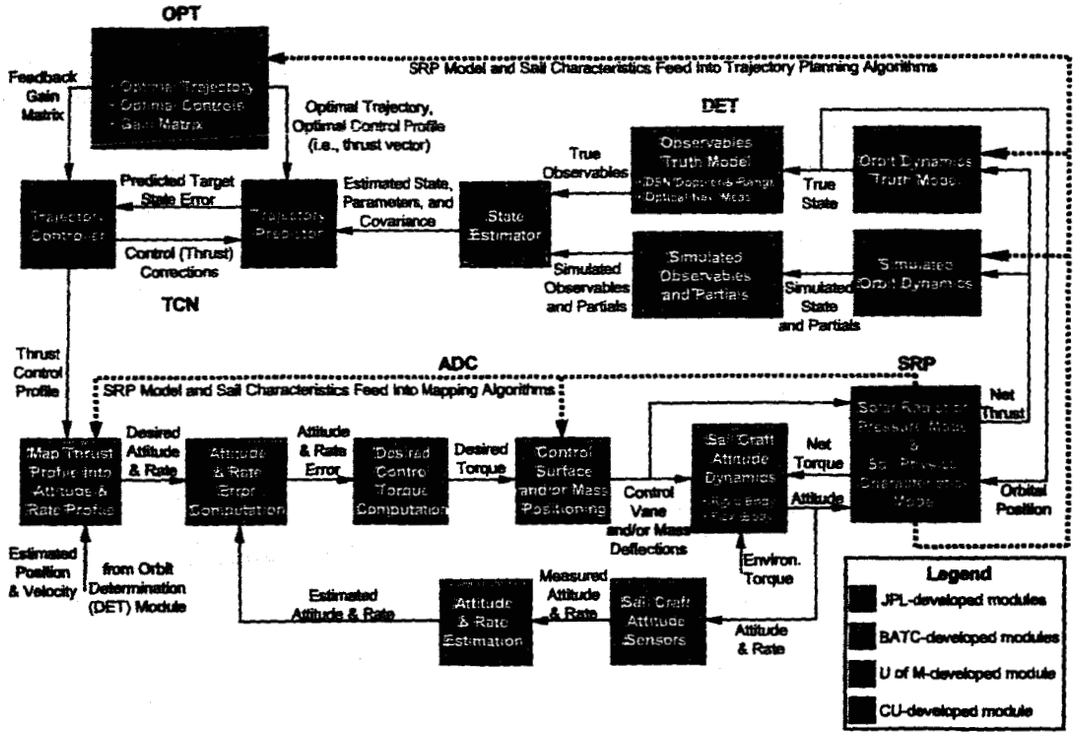

Figure 1. Solar Sail Spaceflight Simulation Software (S5) Functional Block Diagram

Key functions are (i) trajectory optimization to generate the nominal flight path, (ii) trajectory control to correct the actual flight path, (iii) attitude dynamics and control, (iv) solar radiation pressure (SRP) modeling, and (v) orbit determination. Given a nominal trajectory generated by the optimization module, the simulation executes two main loops. A guidance and navigation loop performs orbit determination using net sailcraft thrust computed by the SRP module. In addition, this loop implements trajectory control (i.e., generates desired thrust commands) from the error between estimated and nominal trajectories. The second loop is the attitude control loop, which converts thrust commands from the Trajectory Control (TCN) module into vehicle attitude commands and then executes an attitude feedback control loop.

A series of functional blocks along the bottom of Figure 1 depict the Attitude Dynamics and Control (ADC) module. The first functional block in the ADC Module maps TCN-derived thrust commands into desired sail attitude. This mapping algorithm employs sail physical dimensions and surface reflective characteristics of the SRP model along with sailcraft ephemeris to calculate the required sail attitude to point the thrust vector in the desired direction. In the next ADC

functional block, attitude and angular rate errors are computed by taking the difference between desired and estimated states. The error signals drive a proportional-derivative (PD) or Proportional-Integral-Derivative (PID) compensator stage, identified in the figure as the "Desired Control Torque Computation" block, to produce sailcraft control torque signals. The compensation stage applies user-specified limits to the control torque magnitude to preclude large attitude and rate errors from producing physically unachievable torque commands. Desired control torque signals are transformed into control vane and/or mass/boom assembly gimbal deflection angle commands with an algorithm using SRP model parameters. This transformation procedure occurs in the functional block "Control Surface and/or Mass Positioning". The user may select the sailcraft attitude control architecture: either an articulated control vane implementation or a mass displacement approach (i.e., mass on a gimbaled boom to alter the mass center position relative to the center of pressure). The "Sailcraft Attitude Dynamics block is where true attitude and angular velocity states are generated from torque values produced by the SRP module. These states are sent to the "Sailcraft Attitude Sensor" module, where the attitude measurement process is modeled. Simulated sensor measurements are passed to the "Attitude and Rate Estimation" module, which produces attitude and angular velocity estimates to complete the attitude control feedback loop. Additionally, the S5 ADC module provides dynamics and control modeling for a reaction wheel assembly, attitude control thrusters, and environmental disturbance torque sources.

Solar sail attitude control presents numerous technical issues to be addressed, including actuator selection and sizing, control-structure interaction, required control loop bandwidth and update period, control algorithm development, and sensitivity to SRP modeling errors. Many aspects of sailcraft attitude control and dynamics are discussed in NASA's Solar Sail Technology Working Group final report[12].

Solar sails are often described as gossamer structures. Their required low sail loading and large dimensions produce low frequency, lightly damped, structural dynamic modes. Potential control-structure interaction must be mitigated. One mitigation approach is to select an attitude control loop bandwidth that is significantly (e.g., an order of magnitude) below the lowest predicted structural dynamic modal frequency. Additionally, filter stages can be incorporated into the attitude control compensation, providing additional gain roll-off or notch attenuation at desired frequencies. If advanced finite element modeling and ground-based testing have limited success in predicting on-orbit solar sail structural dynamic frequencies and mode shapes, then on-board system identification methodologies may be justified to support on-orbit tuning of the attitude control system.

Sailcraft GN&C modeling efforts include investigating appropriate attitude control loop update periods, bandwidth, and implementation (e.g., continuous, on-board processing versus periodically uploading ground-based command generation). The need for low bandwidth controllers has been discussed in the context of mitigating control-structure interaction. Accordingly, control loop update periods may be on the order of seconds to minutes, assuming attitude slew maneuvers are executed relatively slowly (and smoothly to avoid structural dynamic excitation). Regarding attitude control implementation, two points of view have emerged. One school of thought holds that solar sail attitude control can be implemented in a fashion akin to a conventional trajectory correction maneuver, where control actuator deflection commands are computed on the ground and updated once a week or so in order to execute trajectory correction commanding. A competing school of thought maintains that continuous, on-board attitude control is the better implementation, offering advantages in disturbance rejection and accommodating modeling errors. Moreover, combining on-board attitude control processing with fault protection logic enables autonomous reconfiguration of redundant actuator and sensor suites in the event of a failure. Controller design issues such as these can be studied using the S5 integrated GN&C simulation tool.

Actuator selection and sizing are important issues being investigated in the sailcraft community. Articulated control vanes on the sail's periphery, mass on a gimbaled boom, mass translation, and actively modifying surface reflective properties (e.g., electro-chromic materials embedded in the sail) are means of changing sailcraft center-of-pressure and/or center-of-mass locations to induce attitude control torque. Conventional attitude control actuators (e.g., reaction wheel assemblies and thrusters) are understood well and mitigate risk if used as functionally redundant control devices for solar sail technology demonstration missions. However, the conventional actuators introduce mass penalties and the inherent mission life limitations of on-board consumables. Scaling solar sail dimensions from relatively modest technology demonstration sailcraft to large operational vehicles favors actuation methods that alter spacecraft center-of-mass and center-of-pressure locations rather than conventional attitude control actuation methods.

This paper compares performance of two competing attitude control architectures that are currently modeled by the S5 ADC module. One implementation employs articulated, reflective control vanes located on the boom tips at the four corners of the sail assembly to provide three-axis attitude control. Essentially, vane articulation produces control torque by altering the vehicle's center-of-pressure location relative to its center of mass position. The second architecture places the spacecraft bus at the end of a boom that is attached to a two-axis gimbal, which produces roll and pitch control torque by moving the vehicle center-of-mass position relative to the center-of-pressure location. The second architecture employs two reflective vanes located at opposing corners of the main sail provide yaw control torque.

Performance of the two competing attitude control implementations is evaluated using a simulated "fly-off". That is to say, each implementation executes an identical sequence of thrust commands from a specific design reference mission (DRM) to drive the attitude control loop. We employ a thrust command trajectory produced by the S5 OPT module to guide the solar sail from the sun-earth L1 point to a sub-L1 point. Performance metrics include thrust direction accuracy, time for maneuver completion, attitude error, and gimbal angle magnitudes.

In addition, this work examines some interesting aspects of the algorithm mapping attitude control torque commands into actuator deflection commands. The mapping algorithm employs a Jacobian pseudo-inverse matrix in a feedback inversion loop. The Jacobian matrix is derived from the SRP model's expression for torque as a function of control vane deflection angles and solar sail attitude relative to the sun-to-sailcraft line. Under certain conditions, the Jacobian matrix has a near-zero minimum singular value, which can result in relatively large changes in vane deflection angle over relatively short time periods. This work considers methodologies aimed at mitigating this effect.

TWO SOLAR SAIL ATTITUDE CONTROL IMPLEMENTATIONS

Figure 2 illustrates a solar sail with four articulated, reflective, control vanes attached to the tips of the sail's support booms. Each control vane rotates about a single axis that is parallel (or nearly parallel) to its support boom, which has the effect of altering the sail's aggregate center of pressure location in the plane of the sail, generating torque about an axis in this plane. Articulating opposing vanes in a coordinated fashion induces a "windmill" torque on the solar sail (i.e., about an axis normal to the plane of the sail). Thus, the vanes can be rotated to produce control torque about all three axes.

Figure 3 depicts an alternative solar sail attitude control implementation, one with a mass/boom assembly attached to a two-axis gimbal that is used to shift the vehicle mass center relative to the main sail's center of pressure. Sailcraft roll (about the x-axis) and pitch (about the y-axis) control torques are produced by gimbaling the mass/boom assembly. Controlling yaw (about the z-axis)

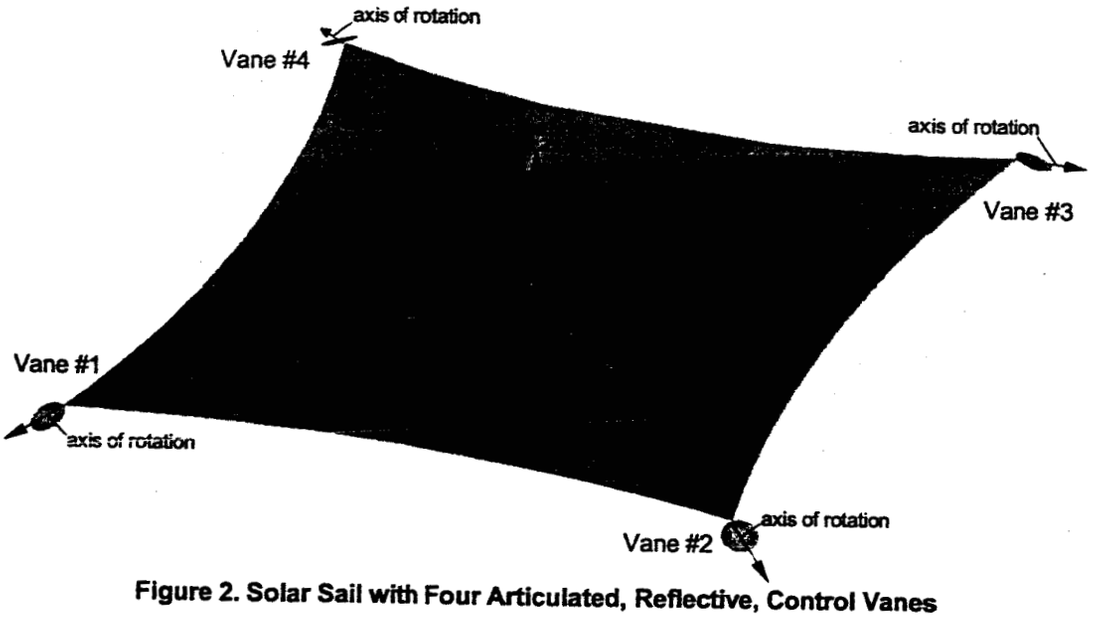

Figure 2. Solar Sail with Four Articulated, Reflective, Control Vanes

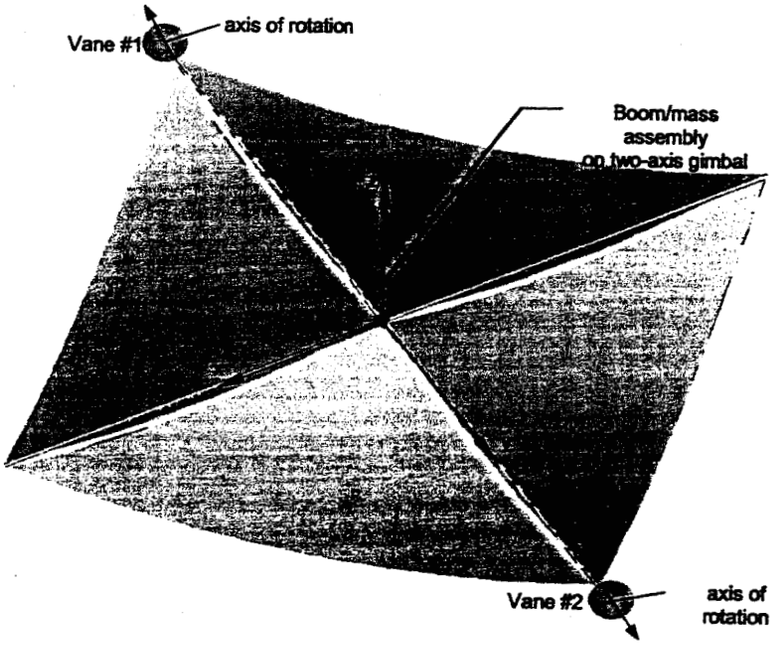

Figure 3. Solar Sail with Gimbaled Mass/Boom and Two Articulated, Control Vanes

is achieved with the two reflective control vanes attached to the tips of the sail's support booms. These opposing control vanes are articulated in a coordinated fashion to generate a "windmill" torque on the solar sail. Thus, this sailcraft attitude control system is also able to produce control torque about all three axes.

Arguments favoring the articulated, reflective, control vane architecture include:

- Conducive to scaling (because the moment arm increases with sail area)
- Three axes of attitude control
- Passive stability by canting the vane back from the plane of the main sail
- Some level of redundancy in the event that one of the four vanes fails
- Potential for thrust modulation (assuming vane area is non-trivial percentage of sail area)

Arguments in favor of gimbaled mass/boom assembly architecture include:

- Large bus mass allows significant shift in vehicle mass center location with relatively small gimbal angles
- Reduced mass at the boom tips decreases vehicle inertia and helps alleviate control-structure interaction

Trade studies must be performed to assess mass and power implications for these competing architectures. Likewise, analysis and testing of control-structure interaction issues must be conducted for these competing approaches.

Attitude Control Actuator Deflection Angle Command Generation

For both attitude control implementations, determining the proper vane and/or boom deflection angles to produce a desired control torque employs an algorithm derived from the SRP model's non-linear expression for torque as a function solar sail attitude relative to the sun-to-vehicle line, sail surface reflective properties, and control vane deflection angles. The attitude control loop generates desired torque from attitude and angular velocity errors using a PD or PID compensator stage. Mapping control torque into vane deflection angles requires inverting the aforementioned non-linear function. The inversion process uses a Jacobian pseudo-inverse matrix inside a feedback inversion loop. A derivation of the former is summarized below.

Eq. (1) represents the nonlinear expression for torque $\boldsymbol{\tau}$ induced on a solar sail as a function of an array of vane deflection angles $\{\theta\}$, vehicle attitude relative to the sun direction vector, and SRP model parameters. (Vehicle attitude and SRP model parameters are not shown explicitly.)

$$\boldsymbol{\tau} = \mathbf{f}(\{\theta\}) \tag{1}$$

Eq. (1) is linearized about the current state (i.e., vehicle attitude and vane deflection angle $\{\theta\}_n$ for the n^{th} update cycle of the attitude control loop) to obtain an expression for the incremental change in torque resulting from an incremental change in the vane deflection state as shown in Eq. (2).

$$\begin{aligned} \delta\boldsymbol{\tau} &= \left[\frac{\partial}{\partial\{\theta\}}\left(\mathbf{f}(\{\theta\})\right)\right]\delta\{\theta\} \\ &= \mathbf{J}\left(\{\theta\}_n\right)\delta\{\theta\} \end{aligned} \tag{2}$$

A linear relationship for vane deflection angle perturbation as a function of torque command perturbation is obtained by calculating the pseudo-inverse of the Jacobian matrix $\mathbf{J}(\{\theta\}_n)$ as shown in Eq. (3). This expression is valid over small variations about the nominal state.

$$\delta\{\theta\} = \mathbf{J}^{\dagger}(\{\theta\}_n)\delta\tau \tag{3}$$

Figure 4 depicts the attitude control loop residing in the integrated S5 GN&C simulation tool. It features a PD compensator stage for generating commanded torque, the algorithm determining control vane deflection commands with the Jacobian pseudo-inverse and feedback inversion loop, the SRP model, and the sailcraft attitude dynamics.

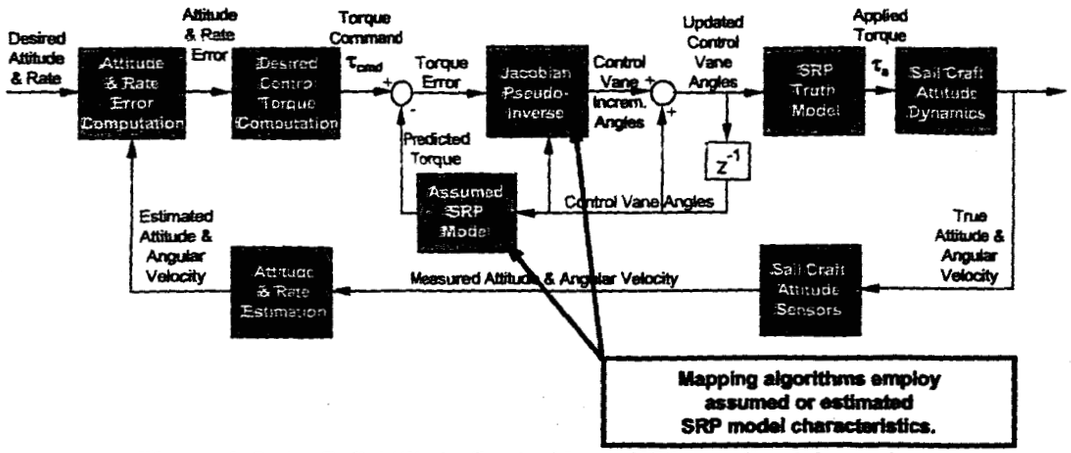

Figure 4. Solar Sail Attitude Control Loop With Feedback Inversion

ATTITUDE CONTROL PERFORMANCE COMPARISON

Attitude control performance between the two competing architectures is evaluated by executing an identical sequence of thrust commands from a specific design reference mission (DRM). We employ a thrust command trajectory produced by the S5 OPT module to guide the solar sail from the sun-earth L1 point to a sub-L1 point. Recall that thrust commands at each time step are mapped into attitude commands by the ADC module, and then the attitude control loop is executed. Performance metrics include thrust direction accuracy, time for maneuver completion, attitude error, and gimbal angle magnitudes. The left-hand pane of Figure 5 illustrates the orbital trajectory of the 285-day transfer from the sun-earth L1 point to the desired sub-L1 point, and the right-hand pane shows the commanded thrust (expressed in a solar system barycentric inertial reference frame). The desired sailcraft attitude that produces the commanded thrust direction is co-plotted with true attitude in Figures 6, 7, and 8. Thrust commands and, thus, desired vehicle attitude are updated once every 24 hours.

Attitude Control Performance for Articulated Vane Implementation

Figure 6 illustrates several performance metrics for the articulated vane sailcraft attitude control architecture during the first 66 hours of the transfer orbit. These plots show that the vehicle completes an attitude slew maneuver and reaches a trim condition after several hours. In the

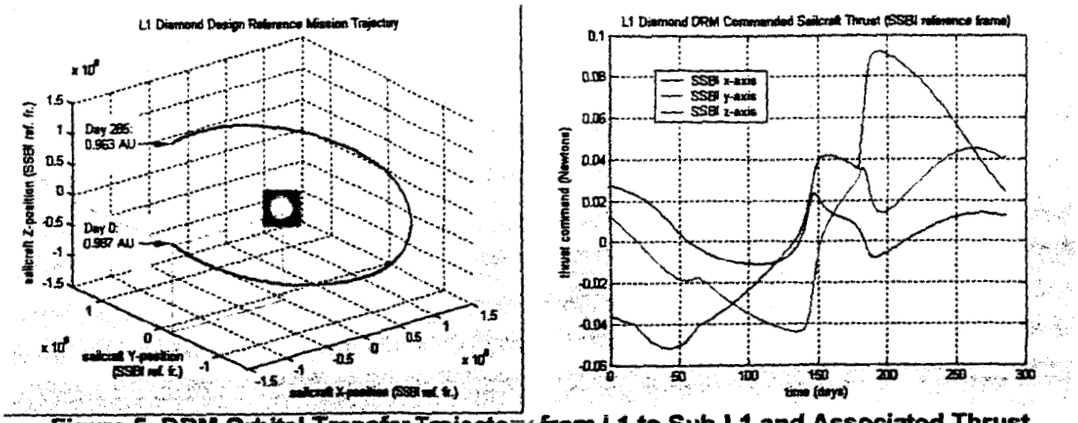

Figure 5. DRM Orbital Transfer Trajectory from L1 to Sub-L1 and Associated Thrust

upper left corner is a plot of the desired (a.k.a., commanded) and true cone angle time histories. (Cone angle is the angle between the thrust vector and the sun-to-sailcraft position vector.) The commanded thrust vector is 45 degrees from the sun-to-sailcraft line, and the true cone angle plot indicates that the vehicle is tracking the commanded thrust direction well. The sailcraft thrust direction is achieved by orienting the solar sail to have a pitch attitude of nearly 50 degrees relative to the sun-to-sailcraft line, as indicated by the plot in the lower right corner. The pitch angle is larger than the cone angle because the solar radiation pressure model assumes the sail surface is not perfectly reflective. (For a planar surface, the thrust vector always lies between the sail surface normal vector and the sun-to-sailcraft position vector, and only a perfectly reflective, planar surface will produce thrust aligned with the surface normal for non-zero cone angles.)

When the thrust command is updated after each 24-hour period, a change in the desired attitude induces the sailcraft control system to move the vanes to a different orientation in order to generate the desired attitude control torque. Once the new desired attitude has been achieved, the vanes settle to a new trim condition that is only a few degrees different from the previous trim condition. Applied solar radiation pressure torque (truth model) matches the commanded torque from the PD compensator well, demonstrating that the control vanes are being articulated in a fashion that generates the desired control torque.

Figure 7 displays long-term performance (125 days) of the articulated vane architecture when implementing the DRM thrust command profile. Among the most prominent features of these plots are the "abrupt" changes in deflection angle, torque, and angular velocity that occur every 24 hours. These "spikes" show the system's transient response to each thrust command update. Command smoothing can be applied, if necessary, to reduce these transients. Plotted results indicate that the true cone angle tracks the desired cone angle well, and this means that the commanded thrust direction is tracked well. Also, applied torque due to solar radiation pressure (truth model) matches the commanded torque well. Control vane articulation angles reach 50 degrees (for vanes #2 and #4), and then their magnitudes begin to diminish after roughly 80 days and the change in deflection angle stabilizes at smaller magnitudes.

Attitude Control Performance for Gimbaled Mass/Boom Assembly Implementation

Next, we turn our attention to the second attitude control architecture, the gimbaled mass/boom assembly. This implementation was subjected to the same thrust command profile as the articulated vane architecture. Figure 8 contains time histories for the gimbaled mass/boom assembly attitude control architecture. The plots indicate the desired cone angle (i.e.,

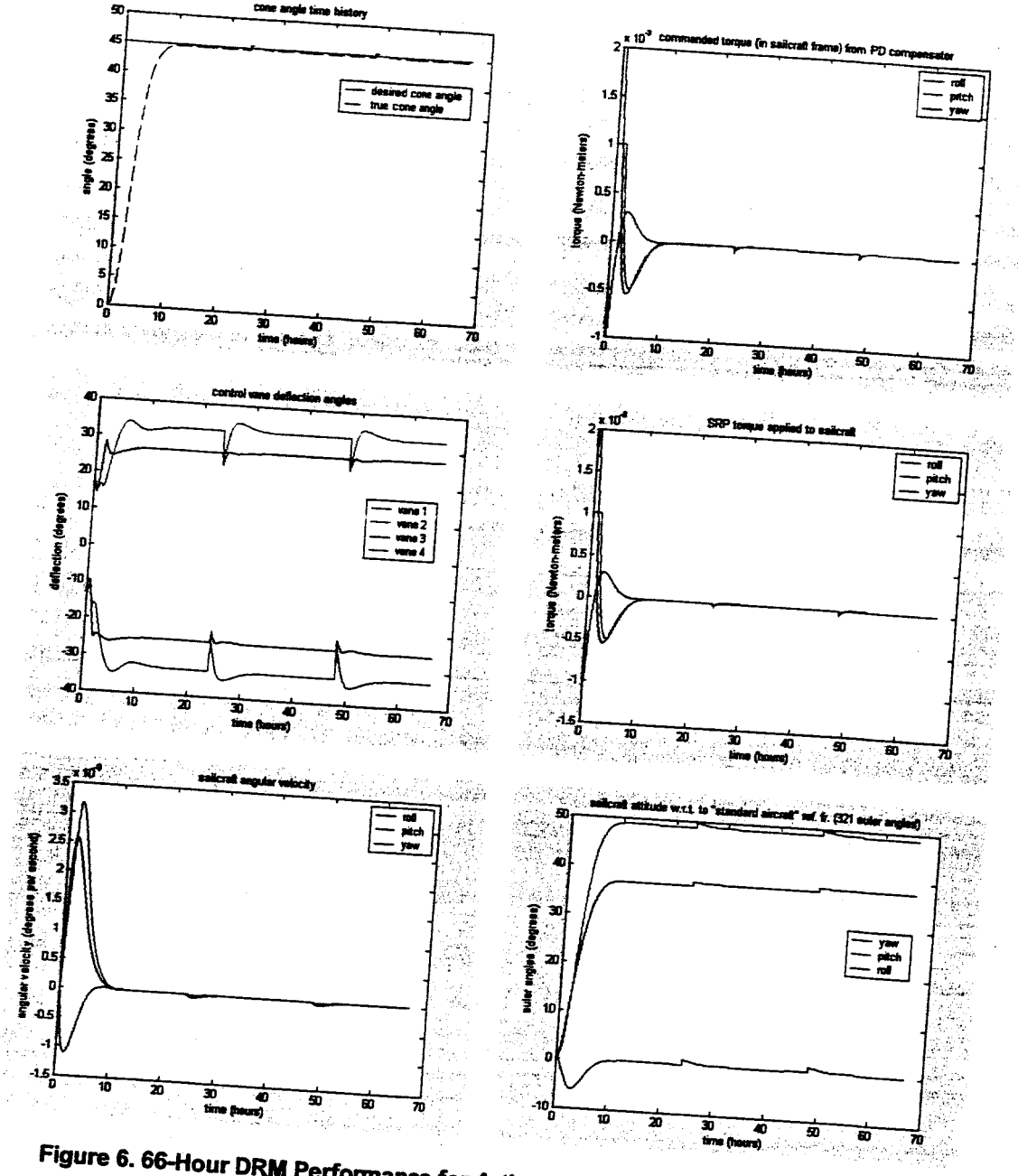

Figure 6. 66-Hour DRM Performance for Articulated Control Vane Implementation

commanded thrust direction) is tracked well. Likewise, solar radiation pressure torque (truth model) matches the commanded torque well, and so boom gimbal angle and vane deflection command generation is being executed correctly. It is interesting to note that the gimbal angle #2 settles to a trim condition of roughly -12 degrees. This relatively small angle is attributable to the bus mass being nearly one-third of the total vehicle mass. For this attitude control architecture, the articulated vanes controlling yaw torque required small deflection angles (i.e., less than one degree) to track the desired yaw attitude trajectory.

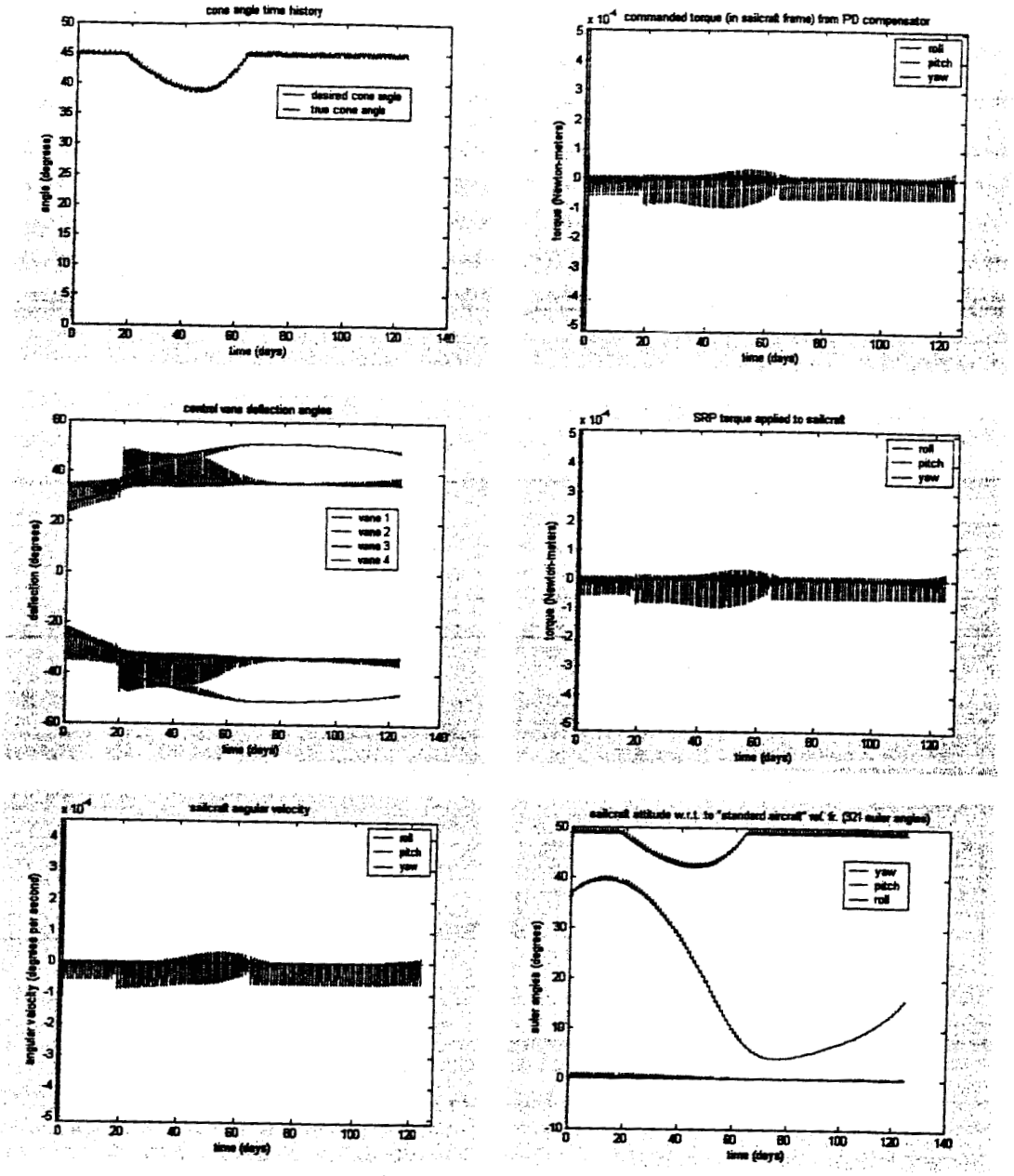

Figure 7. 125-Day DRM Performance for Articulated Control Vane Implementation

Vane Deflection Command Generation and Jacobian Numerical Condition

Simulation results show that, under certain conditions, the command generation algorithm produces large changes in control vane deflection angles over relatively short periods of time. Recall that the deflection angle command generation algorithm relies on a linearized relationship

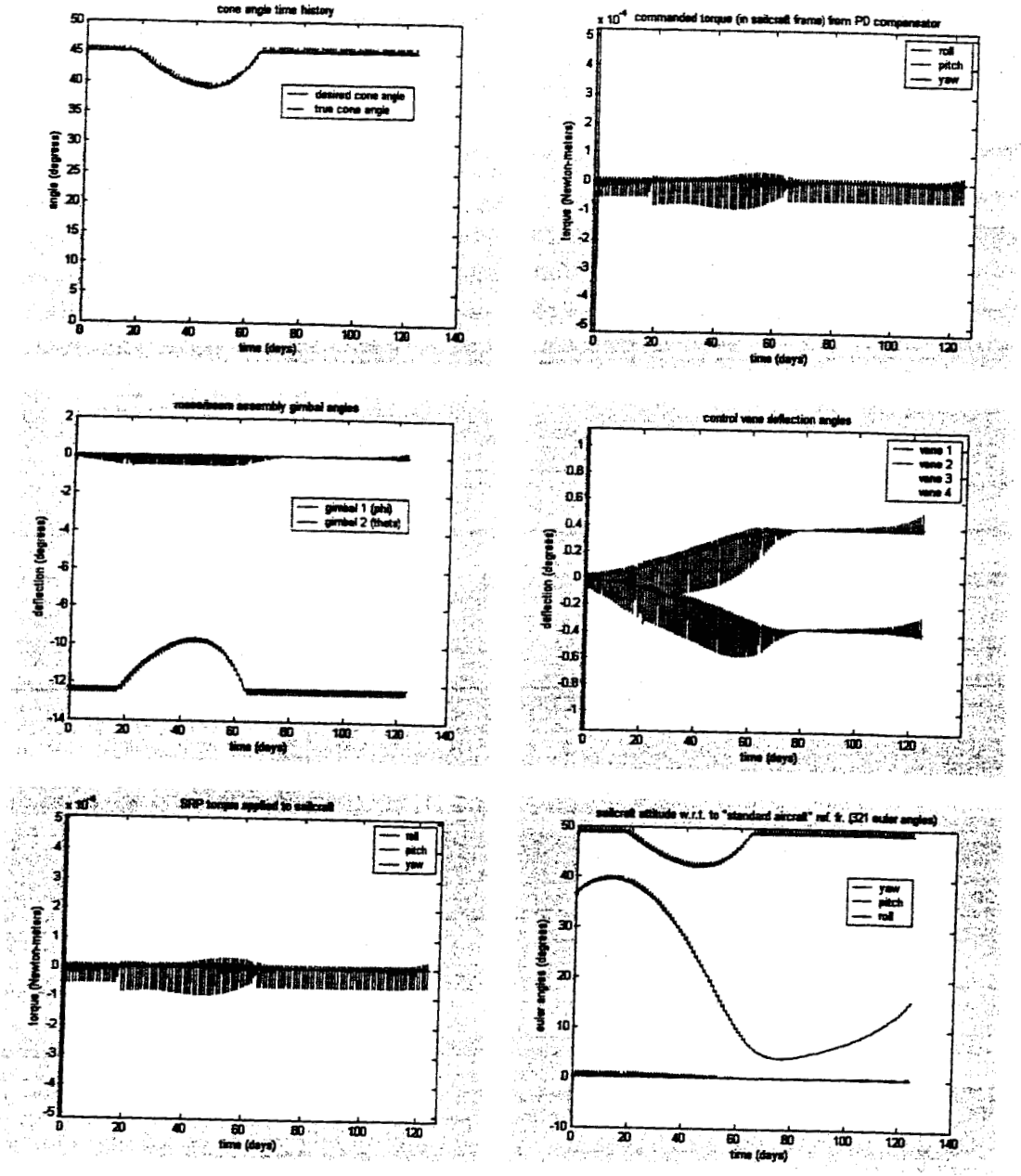

Figure 8. 125-Day DRM Performance for Gimbaled Mass/Boom Implementation

between actuator deflection angle and torque induced by the solar radiation pressure acting on the deflected actuator surfaces. Since the process of mapping a three-element torque command vector into a four-element deflection angle array is an underdetermined problem, an infinite number of solutions exist. If vane deflection angles are allowed to "drift" within this solution set, large deflection angles may result over time. Smaller deflection angle ranges are preferable for two reasons:

- Smaller (or minimum necessary) deflection angles reduce mechanism total travel distance, reducing mechanism wear.
- Control vanes should not expose their "back" side to the sun because (i) the reflective surface is on the "front" side only and (ii) the control law becomes invalid.

Large deflection angle changes are correlated with near-zero reciprocal condition numbers for the Jacobian matrix. That is to say, vane deflection angles tend to experience large changes when the minimum singular value of the Jacobian matrix becomes small because the Jacobian pseudo-inverse (mapping from commanded control torque to desired vane deflection angle) essentially introduces a large gain into the feedback inversion loop.

Consider the contrasts in simulation cases presented in Figures 9 and 10. Figure 9 illustrates articulated vane control architecture performance time histories during the first 12 hours of the DRM case discussed earlier. The figure includes plots of vane deflection angles, commanded change in vane deflection angle, the corresponding ratio of minimum to maximum singular value for the Jacobian matrix, and the error between commanded torque and estimated torque in the feedback inversion loop. For this case, the vane deflection angles reach a steady-state trim condition within several hours, and the commanded change in vane deflection angles is modest (once the start-up transient has been completed). Moreover, the ratio of the minimum singular value to the maximum (a.k.a., reciprocal condition number) does not approach zero. Also, the torque error is small enough for the feedback inversion loop to converge after a single iteration.

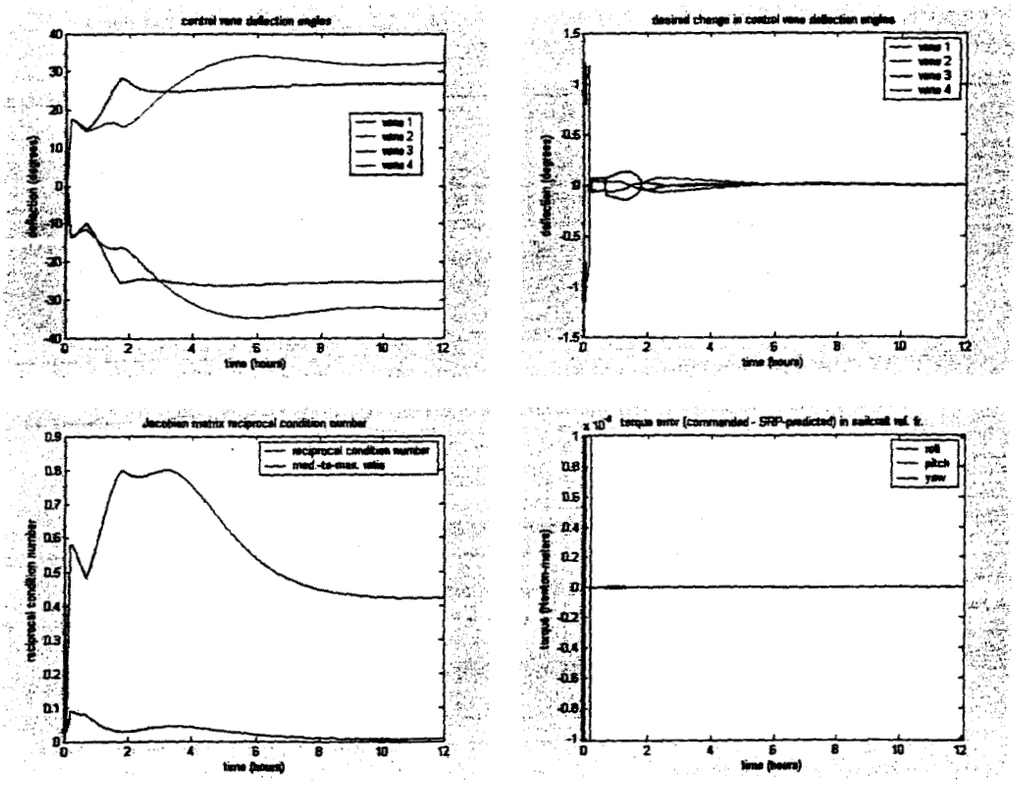

Figure 9. Articulated Vane Control Architecture Performance for Nominal Bandwidth

In contrast, Figure 10 shows the same case except that the control loop bandwidth has been increased by 67%. One impact is that the higher bandwidth boosts the commanded control torque, which alters the vane deflection angle trajectory relative to the lower bandwidth case. More significantly, the reciprocal condition number becomes small just after six hours into the simulation, and the resulting change in vane deflection angles is significant and the transition is not smooth. In this case, vanes #1 and #3 change direction abruptly and reach larger magnitudes (in the vicinity of 40 degrees), while vanes #2 and #4 settle to magnitudes around 10 degrees. Recall that for the lower bandwidth scenario (shown in Figure 9) the vane deflection angles experience relatively smooth transitions and all four vanes settled to deflection angle magnitudes near 30 degrees. In addition, the feedback inversion loop torque error is larger for the scenario shown in Figure 10.

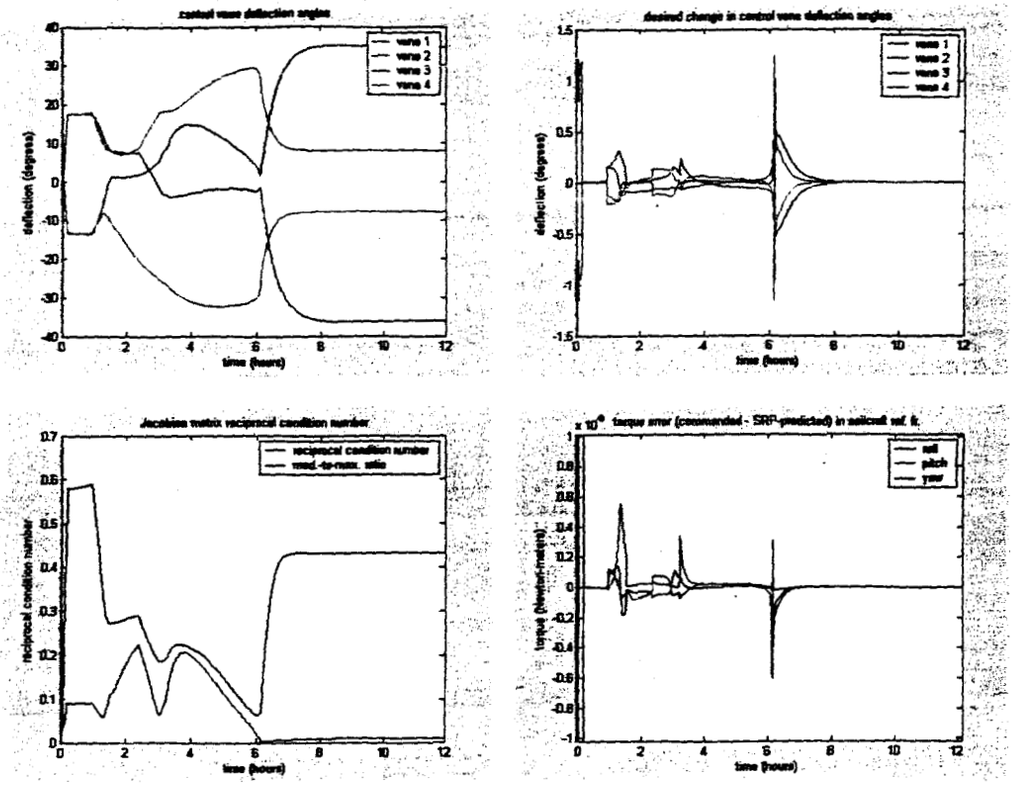

Figure 10. Articulated Vane Architecture Performance for 67% Increase in Bandwidth

One mitigation technique that we have employed to diminish the amplification effect of Jacobian matrices with near-zero reciprocal condition numbers is to adjust the minimum singular value according to the method of Ford and Hall[13]. Figure 11 presents simulation results for the same DRM scenario as shown in Figure 10, except that the Jacobian's minimum singular value is adjusted using the method of Ford and Hall. In this case, time histories are nearly identical to those of Figure 10 until just after 6 hours of simulation time. At that point in time, the singular value adjustment diminishes the large changes in commanded vane deflection angle, and the vanes settle to angles similar to those of Figure 9 (where the reciprocal condition number was not so close to zero).

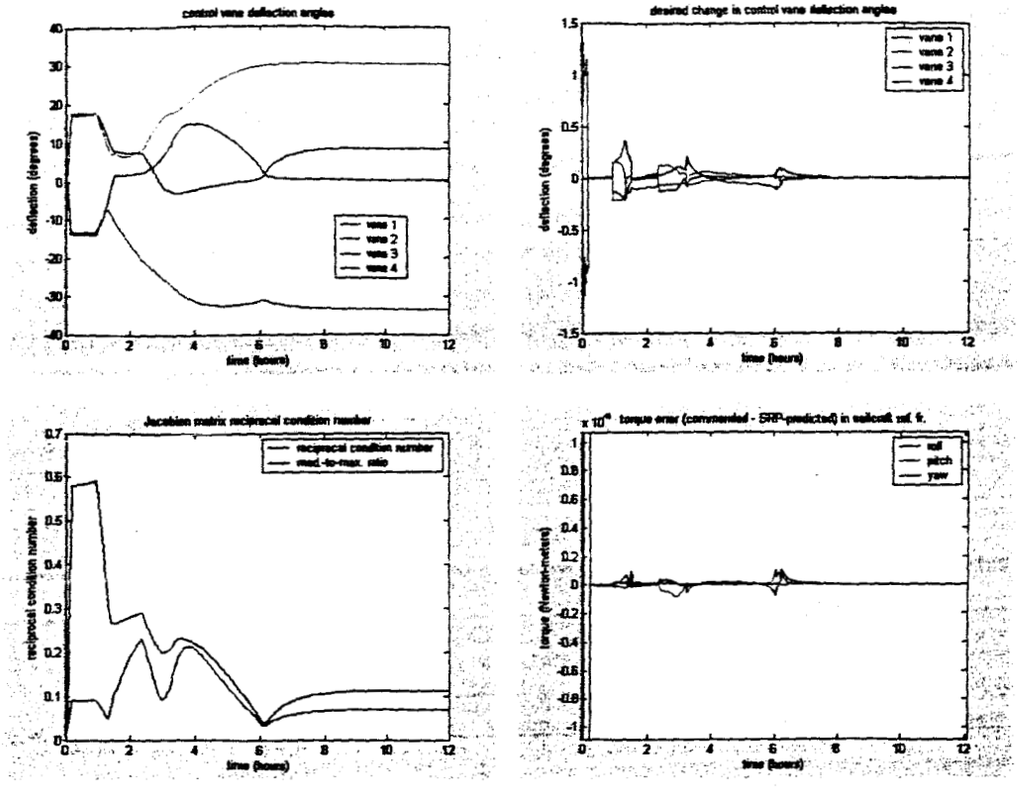

Figure 11. Articulated Vane Architecture Performance for 67% Increase in Bandwidth (Relative to the Case in Figure 9) Improves When Implementing Method of Ford & Hall

The Jacobian matrix is a function of vane deflection angles and main sail attitude relative to the sun-to-sail line. As such, the reciprocal condition number approaches zero for certain combinations of deflection angles as shown in Figures 12 and 13. For instance, Figure 12 shows that the ratio of the smallest to largest singular value approaches zero when certain combinations of vanes have zero deflection angles. Vane #2 being near zero (along with vane #3 being near zero) produces a small minimum singular value no matter what the deflection angle is for vane #1. Similarly, a near-zero deflection angle for vane #1 (along with a small deflection angle for vane #4) yields a near-zero reciprocal condition number. Figure 13 illustrates that the reciprocal condition number is more benign when all four vanes have angles that are away from 0 or 90 degrees, but there are still a few regions in the surface with near-zero minimum singular values. These plots assume sailcraft attitude is such that the main sail normal vector is aligned with sun-to-sailcraft direction vector.

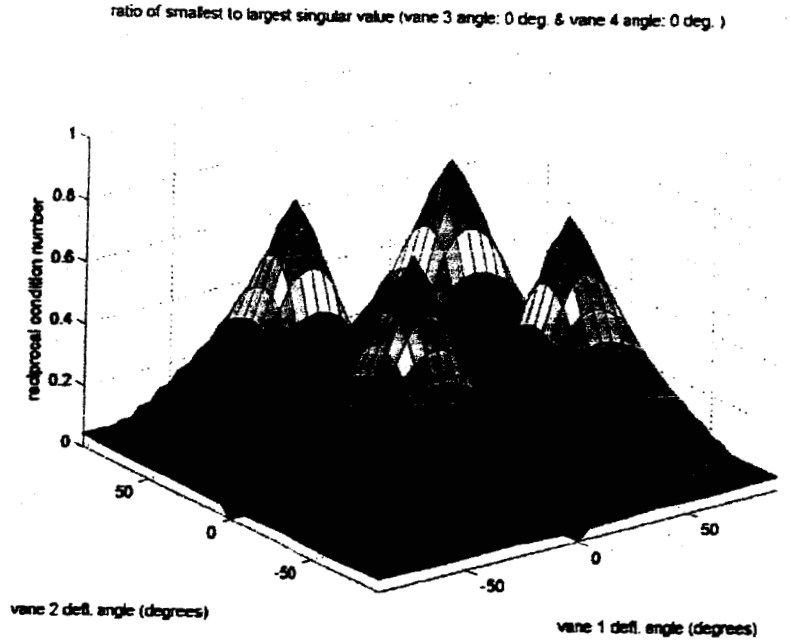

Figure 12. Jacobian Matrix Reciprocal Condition Number Approaches Zero for Control Vane Deflection Angles Near 0° and 90°

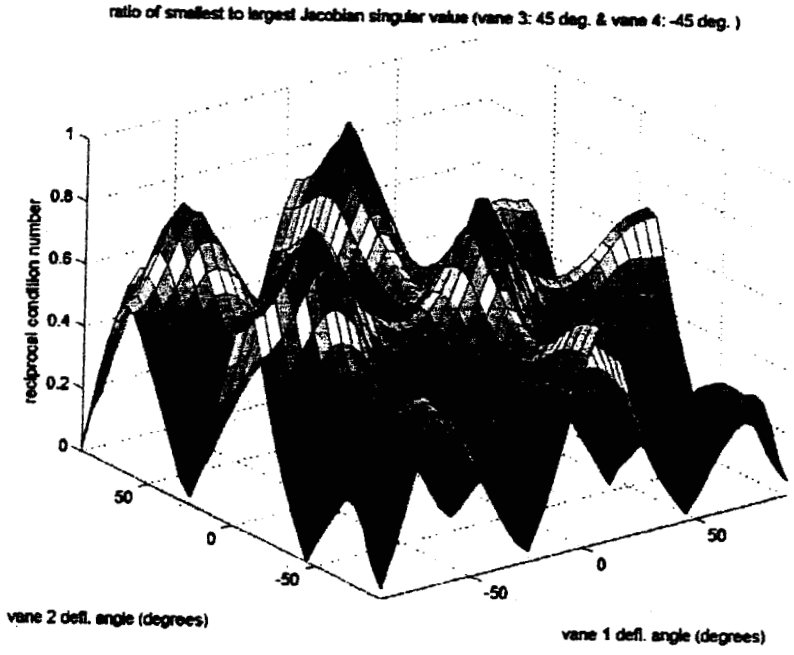

Figure 13. Jacobian Matrix Reciprocal Condition Number Larger for Control Vane Deflection Angles Away from 0° and 90°

MANAGING VANE DEFLECTION ANGLE GROWTH VIA NULL-SPACE LEAKAGE

Although the singularity avoidance of the Jacobian pseudo-inverse provides smooth vane angle solutions, they still drift significantly away from the desired minimum norm set. A promising approach to mitigate this drift is to introduce null-space leakage into the feedback inversion loop. First, we discuss the feedback inversion methodology, and then we describe algorithm modifications (i.e., null-space leakage) designed to counter vane deflection angle growth.

Feedback Inversion Loop

Feedback inversion of the function $\mathbf{f}(\{\theta\})$ produces an argument $\{\theta\}$ that corresponds to a given value $\boldsymbol{\tau} = \mathbf{f}(\{\theta\})$. This is provided by a feedback loop, which iterates to reduce the error between the desired value $\boldsymbol{\tau}$ and an estimate $\hat{\boldsymbol{\tau}}_k = \mathbf{f}(\{\hat{\theta}\}_k)$, using an appropriate update algorithm for $\{\hat{\theta}\}_k$. The function $\mathbf{f}(\{\theta\})$ determines whether an inverse image $\{\theta\}$ exists for any particular $\boldsymbol{\tau}$, and whether these solutions $\{\theta\}$ are unique. The choice of update algorithm determines whether $\{\hat{\theta}\}_k$ converges to a suitable value, and it determines the convergence rate.

In the present case, vane angles provide redundant actuation, so that any three-vector of desired torque $\boldsymbol{\tau}$ (up to some maximum available value) could be provided by a one-dimensional family of four-vector solutions for vane angles $\{\theta\}$. This can be seen by applying the implicit function theorem[14] to produce a one-dimensional solution manifold for each function value $\boldsymbol{\tau}$, when the Jacobian of $\mathbf{f}(\{\theta\})$ has rank three throughout the domain of interest and results in an implicit function constraining the vane angles. This raises the question: which among this family of solutions for $\{\theta\}$ are suitable for solar sail vane deflections?

The first requirement is to limit the vane angles to physically reasonable values. A second criteria would be to limit the change in vane angles from one time step to the next to be as small as possible, so as to limit extraneous motion of the vane gimbals and excitation of structural vibrations.

A common approach to develop a convergent algorithm for the estimates $\{\hat{\theta}\}_k$ is to employ the linear approximation of $\mathbf{f}(\{\theta\})$ in the Newton-Raphson update scheme. Define $\{\tilde{\theta}\}_k$ as the solution error $\{\theta\}$ - $\{\hat{\theta}\}_k$. Write an expression for the torque error as Eq. (4).

$$\begin{aligned}\boldsymbol{\tau} - \hat{\boldsymbol{\tau}}_k &= \mathbf{f}(\{\theta\}) - \mathbf{f}(\{\hat{\theta}\}_k) \\ &= \mathbf{f}(\{\hat{\theta}\}_k) + \mathbf{J}\left(\{\hat{\theta}\}_k\right)\left(\{\theta\} - \{\hat{\theta}\}_k\right) + o\left(\left\|\{\tilde{\theta}\}_k\right\|\right) - \mathbf{f}(\{\hat{\theta}\}_k) \\ &= \mathbf{J}\left(\{\hat{\theta}\}_k\right)\{\tilde{\theta}\}_k + o\left(\left\|\{\tilde{\theta}\}_k\right\|\right)\end{aligned} \tag{4}$$

where $\mathbf{J}\left(\{\hat{\theta}\}_k\right)$ is the Jacobian of $\mathbf{f}(\{\theta\})$ as defined in Eq. (2), and $o(\cdot)$ indicates higher order terms in the Taylor series expansion which go to zero faster than $(\cdot)$. Eq. (4) yields the update

algorithm of Eq. (5), which reduces $\{\tilde{\theta}\}_k$ by stepping in the opposite direction given by $\mathbf{J}(\{\hat{\theta}\}_k)$ to reduce $\tau - \hat{\tau}_k$.

$$\{\tilde{\theta}\}_{k+1} = \{\tilde{\theta}\}_k - \mu\left[\mathbf{J}(\{\hat{\theta}\}_k)\right]^{-1}(\tau - \hat{\tau}_k) \tag{5}$$

Convergence can be analyzed by replacing τ and $\hat{\tau}_k$ by functions of $\{\theta\}$ and $\{\hat{\theta}\}_k$ as shown in Eq. (6).

$$\begin{aligned}\{\tilde{\theta}\}_{k+1} &= \{\tilde{\theta}\}_k - \mu\left[\mathbf{J}(\{\hat{\theta}\}_k)\right]^{-1}\left[\mathbf{J}(\{\hat{\theta}\}_k)\{\tilde{\theta}\}_k + o\left(\|\{\tilde{\theta}\}_k\|\right)\right] \\ &= \left(\mathbf{I}_{4x4} - \mu\left[\mathbf{J}(\{\hat{\theta}\}_k)\right]^{-1}\left[\mathbf{J}(\{\hat{\theta}\}_k)\right]\right)\{\tilde{\theta}\}_k - \mu\left[\mathbf{J}(\{\hat{\theta}\}_k)\right]^{-1} o\left(\|\{\tilde{\theta}\}_k\|\right)\end{aligned} \tag{6}$$

In the absence of the second term on the right, this is an asymptotically stable recursion provided that $0 \le \mu < 1$. An exponential convergence rate can be guaranteed by comparison to the scalar recursion $a_{k+1} = \sigma\, a_k$, where σ equals the maximum eigenvalue of $\left(\mathbf{I}_{4x4} - \mu\left[\mathbf{J}(\{\hat{\theta}\}_k)\right]^{-1}\left[\mathbf{J}(\{\hat{\theta}\}_k)\right]\right)$, which is less than 1 by choosing $0 \le \mu < 1$.

This exponential stability provides robustness to perturbations using Total Stability Theory[15], resulting in convergent errors $\{\tilde{\theta}\}_k$, provided the perturbing second function on the right is made small enough relative to $(1-\sigma)$ by starting $\{\hat{\theta}\}_k$ close enough to a solution $\{\theta\}$. This shows that the recursion is locally asymptotically stable.

Unfortunately, $\left[\mathbf{J}(\{\hat{\theta}\}_k)\right]^{-1}$ does not exist in this application because the Jacobian is a 3 x 4 matrix. Using the pseudo-inverse $\mathbf{J}^{\dagger}(\{\hat{\theta}\}_k)$ results in $\mathbf{J}^{\dagger}(\{\hat{\theta}\}_k)\mathbf{J}(\{\hat{\theta}\}_k)$ with rank 3 (or less). Hence the 4 x 4 matrix $\mathbf{M} \equiv \left(\mathbf{I}_{4x4} - \mu\left[\mathbf{J}^{\dagger}(\{\hat{\theta}\}_k)\right]\left[\mathbf{J}(\{\hat{\theta}\}_k)\right]\right)$ has a maximum singular value equal to one. Therefore, the unperturbed recursion is *not* exponentially stable, and it may be sensitive to small perturbations. Local stability and convergence is no longer guaranteed. In particular, the minimum norm quality of the pseudo-inverse solution may not be obtained in the solution iterates, which can drift along the one-dimensional solution manifold away from the minimum-norm solution.

Feedback Inversion Algorithm Modifications Incorporating Null-Space Leakage

To restrain solution drift along the zero-torque manifold, the feedback inversion algorithm is modified to include a leakage factor P_k. Defining the error $\tilde{\theta}_k = \theta_d - \hat{\theta}_k$ away from a desired set of vane angles θ_d yields the error propagation formula in Eq. (7).

$$\{\tilde{\theta}\}_{k+1} = P_k\{\tilde{\theta}\}_k - \mu\,\mathbf{J}^{\dagger}(\{\hat{\theta}\}_k)(\tau - \hat{\tau}_k) \tag{7}$$

The leakage factor is constructed using orthonormal basis vectors for the subspace orthogonal to the rows of the Jacobian $\mathbf{J}\left(\{\hat{\theta}\}_k\right)$. Scaling coefficients are applied to construction of the leakage factor in order to adjust the speed of leakage of vane deflection errors in the nullspace of $\mathbf{J}\left(\{\hat{\theta}\}_k\right)$. Note that the original algorithm is obtained for updates in the subspace spanned by the rows of $\mathbf{J}\left(\{\hat{\theta}\}_k\right)$, since P_k is an identity operator on that subspace. In contrast, P_k produces a contraction along the nullspace of $\mathbf{J}\left(\{\hat{\theta}\}_k\right)$, keeping drift along the zero torque manifold in check.

Figure 14 illustrates vane deflection angle and sailcraft attitude time histories for two simulation cases, one without null-space leakage in the feedback inversion loop (shown in the plots on the left side) and the second with leakage incorporated into the algorithm (shown in the plots on the right side). The simulation is initialized to model a simple, intuitive geometry in which the commanded thrust is oriented along the sun-to-sailcraft line, the vanes are deflected in a trim condition (i.e., +45° for vane #1 and vane #3 and -45° for vane #2 and vane #4), and a 10° roll error exists in sailcraft attitude. For the case without null-space leakage, the vanes deflect in a manner to correct the attitude error and then settle to within a 0.2° of their initial trim orientation.

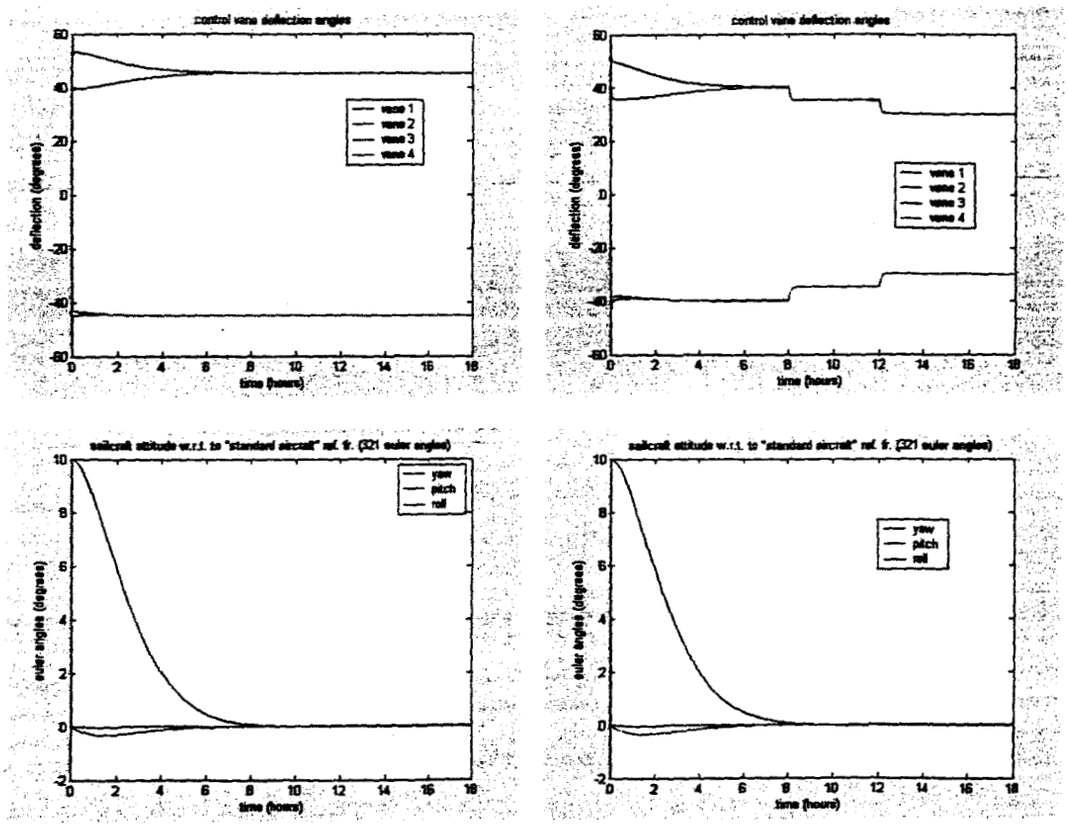

Figure 14. Vane Deflection Angle Time Histories with and without Null-Space Leakage

The trim condition (a.k.a., zero-torque manifold) for this sailcraft geometry is the set of vane deflection angles such that (i) all four have the same magnitude, (ii) deflection angles for vane #1 and vane #3 have the same sign, and (iii) the sign of deflection angles for vane #2 and vane #4 is the negative of that for the other two vanes). For example, this sailcraft-to-sun geometry is

trimmed as well for a vane angle set of +/- 10° as it is for a set of +/- 45°. Thus, the null-space leakage algorithm should drive the vane deflection angles along the zero-torque manifold to a desired set that has smaller magnitude.

The simulation case with null-space leakage is initialized with the vanes' desired trim angles set to +/- 40°. Here, too, the vanes deflect to generate corrective attitude control torque, and then they settle to the desired steady-state trim angle set. Desired angles are changed to a new trim condition of +/-35° after 8 hours of simulation time, and the desired trim condition is set to +/- 30° after 12 hours. Plots demonstrate successful operation of the null-space leakage algorithm in that desired vane deflection angles are achieved while maintaining the correct sailcraft attitude to generate the commanded thrust.

CONCLUSION

The Attitude Dynamics and Control (ADC) module of the Solar Sail Spaceflight Simulation Software (S5) GN&C tool is used to evaluate performance of two solar sail attitude control architectures. One implementation employs four articulated, reflective, control vanes attached to the tips of the sail's support booms to produce three-axes of control torque. A second architecture uses a gimbaled mass/boom assembly to alter the mass center location relative to the center of pressure for roll and pitch control. This architecture produces yaw control torque by articulating two reflective control vanes.

Both attitude control architectures process the same thrust command sequence generated by the S5 OPT module. The thrust commands produce an orbital trajectory guiding the solar sail from the sun-earth L1 point to a sub-L1 point. Simulation results indicate that both attitude control architectures perform well in that the thrust command direction is tracked closely. In addition, the articulated control vane implementation exhibits reasonable deflection angle magnitudes in that trim conditions are less than 50 degrees. Likewise, the gimbaled boom architecture requires relatively small gimbal angle magnitudes to achieve sailcraft attitude producing the commanded thrust directions.

Sailcraft control actuator deflection angles are computed from desired control torque using a feedback inversion loop with a Jacobian pseudo-inverse matrix derived from the SRP model. Large deflection angle changes are correlated with a near-zero minimum singular value for the Jacobian matrix. We demonstrated a promising approach for mitigating this undesirable effect of near-zero reciprocal condition numbers.

Lastly, we examined a means of countering solution drift along the zero-torque manifold by introducing a null-space leakage factor into the feedback inversion loop. Simulation results demonstrate that the leakage algorithm successfully drives vane deflection angles along a simple zero-torque manifold to a desired trim condition. Future research will investigate applying the null-space leakage algorithm to more general sailcraft-to-sun attitude geometries, where the nature of the zero-torque manifold is less obvious than the case study presented herein.

ACKNOWLEDGEMENT

Work documented herein has been performed as part of the Solar Sail Integrated Mission Simulation Tools study, led by the Jet Propulsion Laboratory, California Institute of Technology, under contract with the National Aeronautics and Space Administration's In-Space Propulsion Technologies Office of the Marshall Spaceflight Center. Ball Aerospace & Technologies Corp. and the University of Colorado are under subcontract with the Jet Propulsion Laboratory.

REFERENCES

1) Wright, J.L., *Space Sailing*, Gordon and Breach Science Publishers, 1992.

2) McInnes, C.R., *Solar Sailing: Technology, Dynamics, and Mission Applications*, Springer Praxis Publishing, 1999.

3) Yen, C.-W. L., "Solar Sail Geostorm Warning Mission Design", AAS 04-107, 14th AAS/AIAA Space Flight Mechanics Conference, Maui, Hawaii, February 8 – 12, 2004.

4) Sauer, C.G., "The L1 Diamond Affair", AAS 04-278, 14th AAS/AIAA Space Flight Mechanics Conference, Maui, Hawaii, February 8 – 12, 2004.

5) West, J.L., "The Geostorm Warning Mission: Enhanced Opportunities Based on New Technology", AAS 04-102, 14th AAS/AIAA Space Flight Mechanics Conference, Maui, Hawaii, February 8 – 12, 2004.

6) Murphy, D., Trautt, T., McEachen, M., Messner, D., Laue, G., and Gierow, P., "Progress and Plans for System Demonstration of a Scalable Square Solar Sail", AAS 04-105, 14th AAS/AIAA Space Flight Mechanics Conference, Maui, Hawaii, February 8 – 12, 2004.

7) Bladt, J., Lawrence, D., and Ward, L., "Solar Sail Attitude Control Sensitivity to Solar Radiation Pressure Model Accuracy", AAS 04-282, 14th AAS/AIAA Space Flight Mechanics Conference, Maui, Hawaii, February 8 – 12, 2004.

8) Derbes, B., Lichodziejewski, D., and Veal, G., "A 'Yank and Yaw' Control System for Solar Sails", AAS 04-284, 14th AAS/AIAA Space Flight Mechanics Conference, Maui, Hawaii, February 8 – 12, 2004.

9) Wie, B., Murphy, D., Paluszek, M., and Thomas, S., "Robust Attitude Control System Design for Solar Sails, Part I: Propellantless Primary ACS", AIAA-2004-5010, AIAA Guidance, Navigation, and Control Conference, Providence, Rhode Island, August 16 – 19, 2004.

10) NASA Research Announcement, New Millennium Program Space Technology-9, NNH04ZSS002N, August 25, 2004.

11) Ellis, J., Lisano, M., Wolff, P., Evans, J., Bladt, J., Scheeres, D., Rios-Reyes, L., Lawrence, D., "A Solar Sail Integrated Simulation Toolkit", AAS 04-283, 14th AAS/AIAA Space Flight Mechanics Conference, Maui, Hawaii, February 8 – 12, 2004.

12) Wie, B., "Dynamic Modeling and Attitude Control of Solar Sail Spacecraft", NASA Solar Sail Technology Working Group (SSTWG) Final Report, JPL Contract No. 1228156, January 10, 2002.

13) Ford, K. and Hall, C., "Singular Direction Avoidance Steering for Control-Moment Gyros", Journal of Guidance, Control, and Dynamics, Vol. 23, No. 4, July - August 2000.

14) Spivak, M., *Calculus on Manifolds*, Benjamin/Cummins Publishers, 1965.

15) Anderson, B.D.O., Bitmead, R.R., Johnson, C.R. Jr., Kokotovic, P.V., Kosut, R.L., Mareels, I.M.Y., Praly, L., Riddle, B.D., *Stability of Adaptive Systems*, MIT Press, 1986.